Mehran University Research Journal of Engineering and Technology

https://doi.org/10.22581/muet1982.2203.18

2022, 41(3) 175-184

# Integrated representation for discrete Fourier and wavelet transforms using vector notation

Tariq Javid [a,*], Muhammad Faris [a], Arshad Aziz [b], Pervez Akhtar [c]

[a] *Department of Biomedical Engineering, Faculty of Engineering Sciences and Technology, Hamdard University, Karachi Pakistan*

[b] *Department of Electronic and Power Engineering, National University of Sciences and Technology, Karachi Campus, Pakistan*

[c] *Department of Electrical Engineering, Sir Syed University of Engineering and Technology, Karachi Pakistan*

[*] Corresponding author: Tariq Javid, Email: tariq.javid@hamdard.edu.pk

Received: 23 August 2019, Accepted: 30 November 2021, Published: 01 July 2022

KEYWORDS

Convolution

Correlation

Data fusion

Data merging

Discrete Fourier Transform

Discrete Wavelet Transform

ABSTRACT

Many mathematical operations are implemented easily through transform domain operations. Multiple transform domain operations are used independently in large and complex applications. There is a need to develop integrated representations for multiple transform domain operations. This paper presents an integrated mathematical representation for the discrete Fourier transformation and the discrete wavelet transformation. The proposed combined representation utilizes the powerful vector notation. A mathematical operator, called the star operator, is formulated that merges coefficients from different transform domains. The star operator implements both convolution and correlation processes in a weighted fashion to compute the aggregated representation. The application of the proposed mathematical formulation is demonstrated successfully through merging transform domain representations of time-domain and image-domain representations. Heart sound signals and magnetic resonance images are used to describe transform-domain data merging applications. The significance of the proposed technique is demonstrated through merging time-domain and image-domain representations in a single-stage that may be implemented as the primary processing engine inside a typical digital image processing and analysis system.

## 1. Introduction

The use of transformations is ubiquitous in almost all scientific disciplines and especially prominent in science, technology, engineering, and mathematics (STEM) disciplines. Signals (1D) and images (2D signals) are decomposed into a linear combination of basic waveforms for analysis [1-4]. The frequency-domain representation achieved by the discrete Fourier transform (DFT) offers an intuitive way to analyse time domain and image domain representations. The image domain refers to the spatial domain. Many mathematical operations become easier to implement in the frequency domain. The wavelet representation [5-6] achieved by the discrete wavelet transform (DWT) provides a versatile alternative to the frequency domain representation.

A general transform-based signal or image processing approach transforms a time domain or image domain representation into a transform domain representation, See Fig. 1. The motivation to use a transform domain approach is its simplicity to implement computationally expensive time domain or image domain mathematical operations by the frequency domain or wavelet domain alternatives. The Fourier methods, however, do not perform well to analyse signals and images that have significant frequency content variations. The wavelet techniques provide an elegant, computationally efficient, and flexible solution to this problem [1, 7].

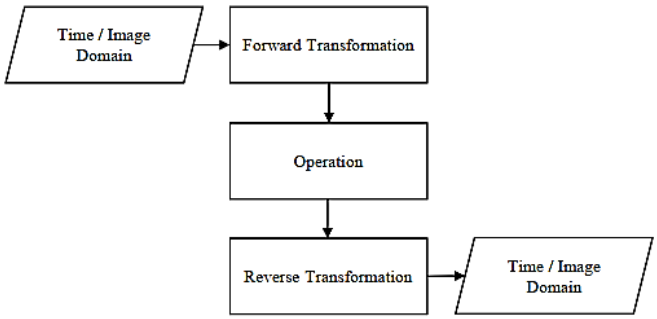


**Fig. 1.** General transform-based signal and image processing approach

A review of research literature on integrated transform domain approaches for data merging (fusion) revealed that generally, these approaches are implemented in either hybrid models or multi-model [8]. The research contributions using data fusion models include the robust watermarking scheme [9] and signature verification [10]. Other closely related contributions in the research literature that unified both DFT and DWT include compressed sensing [11-13] and defect detection [14]. These approaches use transform domain operations for pre-processing and post-processing tasks. The research contributions in the literature are based on the use of frequency domain and wavelet domain operations in separate stages of the techniques [15-17].

The proposed approach in this paper is based on the development of an operation, called the star operator, based on the convolution and correlation processes that are central to both DFT and DWT computations [18], [19]. There are quite a few research pointers found in the literature towards the development of a combined Fourier and wavelet representation [20]. This work is different as the powerful vector notation is used to develop the mathematical expression. Furthermore, the developed algorithms have the inherent ability to merge time domain and image domain representations.

This research proposes a joint mathematical representation for both DFT and DWT through the development of an integrated Discrete Fourier Wavelet Transformation (DFWT) framework. The developed DFWT framework uses the powerful vector space notation in the formulation of the integrated mathematical expression. The application of developed representation is presented through merging: heart sound signals and transform domain coefficients of example magnetic resonance imaging (MRI) image. Figures 2 and 3 show the normal heart sound signal and the example MRI image, respectively.

The paper layout is as follows. Mathematical fundamentals, the star operator, and the integrated DFWT framework are presented in Section 2. The developed mathematical framework and proposed star operator to merge transform domain coefficients are applied and discussed in Section 3. The paper concludes in Section 4 with anticipated future research directions.

## 2. Materials and Methods

### *2.1 Mathematical Fundamentals*

The notation used in this section is based on mathematical expressions in [1], [21]. A discrete signal, $x_n$, is a sampled version of an analog signal, $x(t)$, where $n \in \mathbb{Z}$ and $t \in \mathbb{R}$. A discrete image matrix, $A$, with elements, $a_{rs} = f(x_s,y_r)$, is a sampled version of an analog image, $f(x,y)$, where, $\{r,s\} \in \mathbb{Z}$ and $\{x,y\} \in \mathbb{R}$. A discrete signal or image is mathematically represented and algebraically manipulated in the transform domain. The transform domain representation is obtained by the application of a mathematical operator on an input discrete signal or image. A digital version of discrete counterpart is used for computer storage and processing.

Vector space provides a natural mathematical framework for signal and image analysis. A discrete signal or image may be viewed as an element of a vector space $V$. The vector space $L^2(\mathbb{N})$ contains 1D signals of the form $x_k$ with $k \geq 0$ and satisfies $\Sigma_k |x_k|^2 < \infty$. The $M \times N$ matrix $MAT_{M,N}(\mathbb{R})$ forms an appropriate model that corresponds to a discrete image with elements $a_{rs} \in \mathbb{R}$ such that $0 \leq r \leq m-1$ and $0 \leq s \leq n-1$, where $\{m, n\} \in \mathbb{N}$. The sequence of discrete basic waveforms is denoted by $E_{N,K} = E_k$ with $m$th component is given by $e^{2\pi ikm/N}$, where $k \in \mathbb{Z}$, $N$ is the sampling rate, and $0 \leq m \leq N-1$. Discrete basic waveforms for images take the form of $m$ x $n$ rectangular arrays (2D signals) or matrices with elements in $E_{m,n,k,l} = E_{k,l}$.

A set $S$ with members $e_k$ such that $e_k = 1$ in $k$th position and zero elsewhere is the standard orthogonal bases as $(e_j, e_k) = 0$, when $j \neq k$. Any 1D signal, $v \in V$, can be expressed as $\Sigma_k \alpha_k v_k$, where $\alpha_k = (v, v_k)/(v_k, v_k)$. If a set is orthonormal, then $\alpha_k = (v, v_k)$. This leads to the following inverse discrete Fourier transform (IDFT) formulas (Eqs. 1 and 2) for 1-D signal $X \in \mathbb{C}^N$ and 2D signal $\hat{A} \in MAT_{M,N}(\mathbb{C})$ [1].

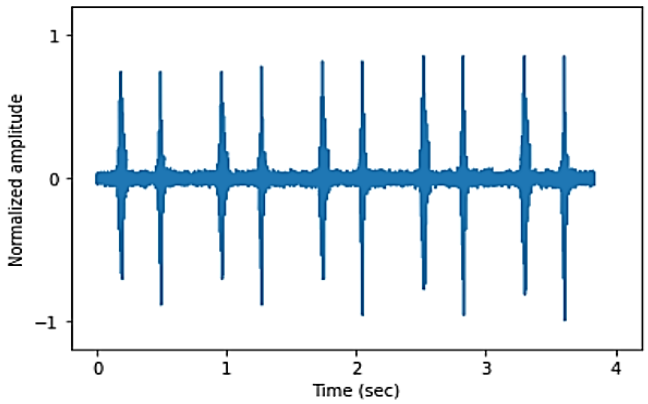


**Fig. 2.** A normal heart sound signal with 8012 Hz sampling frequency and 30745 data points

$$\mathbf{x} = \text{IDFT}(\mathbf{X}) = \frac{1}{N}\sum_{k=0}^{N-1}(\mathbf{x}, \mathbf{E}_k)\mathbf{E}_k \tag{1}$$

$$\mathbf{A} = \text{IDFT}(\hat{\mathbf{A}}) = \frac{1}{MN}\sum_{k=0}^{M-1}\sum_{l=0}^{N-1}(\mathbf{A}, \mathbf{E}_{k,l})\mathbf{E}_{k,l} \tag{2}$$

Where, $0 \leq k \leq N$ -1 for 1D case, and $0 \leq k \leq M-1$ and $0 \leq l \leq N-1$ for 2D case.

The discrete Fourier transform (DFT) of $x \in \mathbb{C}^N$ is the 1D signal $X \in \mathbb{C}^N$ with components are given in Eq. 3.

$$X_k = (\mathbf{x}, \mathbf{E}_k) \tag{3}$$

Where $k \geq 0$.

The IDFT has components are given in Eq. 4.

$$x_k = \frac{(\mathbf{X}, \mathbf{E}_k)}{N} \tag{4}$$

Where $k \geq 0$.

The two-dimensional DFT of **A**, denoted by $\hat{\mathbf{A}}$ has components are given in Eq. 5.

$$\hat{a}_{k,l} = (\mathbf{A}, \mathbf{E}_{k,l}) \tag{5}$$

Where $k, l \geq 0$.

The two-dimensional IDFT of $\hat{\mathbf{A}}$ has components are given in Eq. 5.

$$a_{r,s} = \frac{(\hat{\mathbf{A}}, \mathbf{E}_{k,l})}{MN} \tag{6}$$

Where $k, l, r, s \geq 0$.

The $J$-level orthogonal discrete wavelet transform (DWT) of $x \in \mathrm{R}^N$ has components $a_k^{(J)}, \beta_k^{(J)}, \ldots, \beta_k^{(J)}$ (Eq. 7) [1, 21]

$$\alpha_k^{(J)}, \beta_k^{(l)} = (\mathbf{x}, \mathbf{E}_{\alpha,J}), (\mathbf{x}, \mathbf{E}_{\beta,l}) \tag{7}$$

Where $1 \leq l \leq \mathrm{J}$.

The inverse discrete wavelet transform (IDWT) has components are given in Eq. 8.

$$x_k = \frac{(\alpha_k^{(J)}, \mathbf{E}_{\alpha,J}) + (\beta_k^{(l)}, \mathbf{E}_{\beta,l})}{\sqrt{N}} \tag{8}$$

The $J$-level two-dimensional orthogonal DWT of **A** has components are given in Eq. 9.

$$\alpha_k^{(J)}, \beta_k^{(l)^i} = (\mathbf{A}, \mathbf{E}_{\alpha,J}), (\mathbf{A}, \mathbf{E}_{\beta,l}^i), \tag{9}$$

Where $i \in$ {horizontal, vertical, diagonal} details.

The two-dimensional IDWT has components are given in Eq. 10.

$$a_{r,s} = \frac{(\alpha_k^{(J)}, \mathbf{E}_{\alpha,J}) + (\beta_k^{(l)^i}, \mathbf{E}_{\beta,l}^i)}{\sqrt{MN}} \tag{10}$$

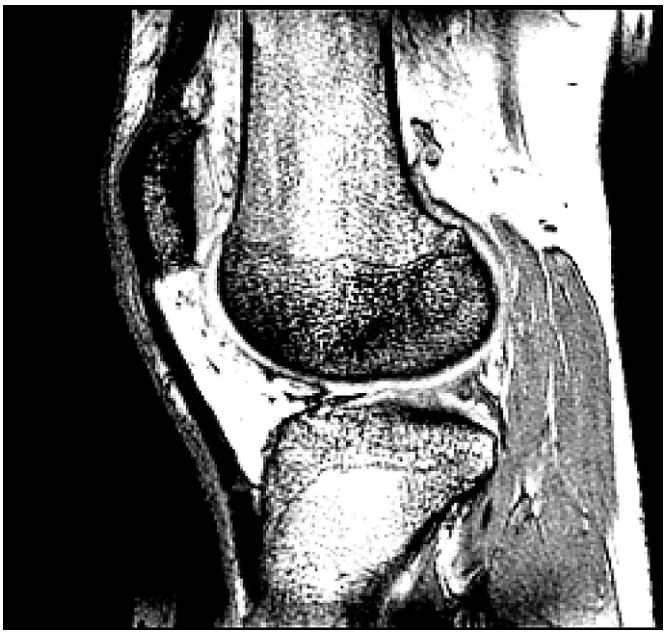

**Fig. 3.** The magnetic resonance image of ankle

The convolution process is the heart of DFT and DWT computations. The steps in standard convolution operation are fold, shift, multiply, and add. These operations are repeatedly used in the convolution process. Use of 2D signals simplifies the implementation of convolution process. Mathematically, this is given as Eq. 11.

$$H * x = \begin{bmatrix} h_0 & h_{N-1} & \cdots & h_1 \\ h_1 & h_0 & \cdots & h_2 \\ \vdots & \vdots & \ddots & \\ h_{N-1} & h_{N-2} & \cdots & h_0 \end{bmatrix} \begin{bmatrix} x_0 \\ x_1 \\ \vdots \\ x_{N-1} \end{bmatrix} \quad (11)$$

Correlation is helpful to measure the similarity between signals or images with its time or frequency delayed version. The correlation process consists of multiple steps including shifting, multiplying, and addition. The correlation process for two different length signals is implemented by making length of smaller signal equal to the length of larger signal. This operation is usually accomplished by zero padding.

*2.2 The Star Operator*

The star operator ($*$) is defined to merge matrices of different sizes as Eq. 12.

$$S_{mn} = A_{mn} \star B_{pq} = \gamma C_{mn} \quad (12)$$

Where the matrix $B_{pq}$ has less number of rows and columns as compared to matrix $A_{mn}$, $\gamma = pq/mn \leq 1$, and $C_{mn}$ is obtained as Eq. 13.

$$\acute{C} = \acute{A} + \omega_i \acute{B} \quad (13)$$

Where $\omega_i$ is the correlation vector, $\acute{A}$ is an extension of $A$, and $\acute{B}$ is an extension of $B$, See Algorithms 1 and 2. The number of members in the correlation vector are $mn - pq + 1$ and the size of matrix $\acute{B}$ is $mn$ $(mn - pq + 1)$. To merge three matrices, Eq. 14 is used.

$$A \star (B_1, B_2) = \gamma_1((\gamma_2(A \star B_1)) \star B_2) \quad (14)$$

Where the matrix $B_2$ has less number of rows and columns as compared to matrix $B_1$. A generalization of the star operator is as Eq. 15.

$$A \star (B_1, \ldots, B_J) = \gamma_1((\gamma_J(A \star B_1)) \star \cdots \star B_J) \quad (15)$$

The vector notation enabled merging of 1D signals and 2D signals, See Algorithms 1 and 2, respectively. The inputs to Algorithm 1 are signals. Both input signals $A_m$ and $B_p$ are represented in the form of $a$ and $b$, respectively. To ensure, the input signals have the required characteristics; parameters $\gamma \leq 1$ and $\Delta \geq 1$ are computed. Next, extensions $\acute{A}$ and $\acute{B}$ for input signals are computed. The correlation vector $\omega_i$ is computed between $a$ and each column of $\acute{B}$. Then, Eq. 13 is used to compute the $\acute{C}$ matrix. The C matrix is obtained through norm of each column of $\acute{C}$. Finally, the $S$ matrix is computed by multiplying $\gamma$ and C. In a similar manner, the input $A_{mn}$ and $B_{pq}$, representing image data, are merged using the procedure in Algorithm 2.

**Algorithm 1**

Star Operator for Merging 1D Signals

Require: 1D Signals: $A_m$, $B_p$

Ensure: Merged 1D Signal: $S_m = A_m * B_p$
1: Convert input signals to 1D signal form: $a$, $b$
2: Compute: $\gamma = p/m \leq 1$
3: Compute: $\Delta = (m - p) \geq 1$
4: Generate extension signal $\acute{A}$:
5: Initialize signal $\acute{A}_{(m\,(\Delta+1))}$ with all columns equal to $a$
6: Generate extension signal $\acute{B}$:
7: Initialize signal $\acute{B}_{(m\,(\Delta+1))}$ with zero element values
8: Fill each column of $\acute{B}$ with values from $b$
9: Each successive column of $\acute{B}$ contains rotated version
10: Compute $\omega_i \in \omega_{(\Delta+1)}$ as correlation between $a$ and each column of $\acute{B}$
11: Compute: $\acute{C} = \acute{A} + \omega_i \acute{B}$
12: Compute: $C$ as vector norm of each row of $\acute{C}$
13: Compute: $S = \gamma C$

In general form, the star operator is implemented by organizing matrices in descending order. Consider the Magic square function in MATLAB. The scaled, rounded version of the result obtained by merging seventh-order

and fifth-order magic square functions using (13) is given as under.

$$\begin{bmatrix} 30 & 38 & 47 & 1 & 11 & 20 & 28 \\ 37 & 46 & 7 & 9 & 19 & 28 & 29 \\ 45 & 6 & 8 & 18 & 26 & 36 & 37 \\ 5 & 14 & 15 & 25 & 35 & 36 & 45 \\ 13 & 15 & 24 & 33 & 42 & 44 & 5 \\ 21 & 23 & 32 & 41 & 43 & 5 & 13 \\ 22 & 30 & 39 & 49 & 3 & 12 & 20 \end{bmatrix}$$

Where $\gamma = 25/49$ and the correlation has following 25 members.

$$\begin{bmatrix} -0.0854 & +0.0146 & -0.0458 & +0.0915 & -0.0345 \\ -0.1079 & -0.0134 & +0.0686 & -0.0832 & +0.0480 \\ -0.0889 & -0.0320 & -0.0355 & +0.0223 & +0.1011 \\ -0.1284 & -0.1239 & +0.1229 & +0.0952 & +0.0957 \\ -0.1883 & +0.0327 & +0.0312 & +0.1458 & +0.1317 \end{bmatrix}$$

The scaled, rounded version of the result obtained by merging seventh-order, fifth-order, and third-order magic square functions using (14) is given as under.

$$\begin{bmatrix} 30 & 38 & 46 & 01 & 12 & 21 & 28 \\ 37 & 45 & 07 & 09 & 20 & 28 & 29 \\ 45 & 06 & 08 & 18 & 27 & 37 & 37 \\ 06 & 14 & 15 & 25 & 36 & 37 & 45 \\ 13 & 15 & 24 & 33 & 43 & 44 & 06 \\ 21 & 23 & 32 & 41 & 43 & 06 & 14 \\ 22 & 30 & 39 & 49 & 03 & 13 & 20 \end{bmatrix}$$

Where $\gamma_2 = 25/49$ and $\gamma_1 = 9/49$. Some typical cases of the star operator are presented below.

*2.2.1 Case – I*

Consider $C = A_{mn} * B_{pq}$ with $A = 0$ and/or $B = 0$. The star operator, introduced in this work, is defined only for non-zero input matrices.

*2.2.2 Case - II*

Consider $C = A_{mn} * B_{pq}$ with $m = p$, $n = q$. The correlation between a seventh-order magic square function and two merged seventh-order magic square functions is 0.9998. The value is one if scaling and rounding effects are removed.

*2.2.3 Case - III*

Consider $C = A_{mn} * B_{pq}$ with $m = 2lp$, $n = 2lq$. Consider $l = 2$, therefore, $p = m/4$, $q = n/4$; for $m = n = 16 \Rightarrow p = q = 4$. The correlation between the result of merging sixteenth-order and fourth-order magic functions; and the sixteenth-order magic square function is one.

*2.2.4 Case - IV*

Consider $C = A * (B_1, B_2, \ldots, B_J)$ with $A = \alpha_k^{(J)}$ and $B_i = \beta_k{}^{(l)^i}$. Consider wavelet decomposition of thirty-secondth-order magic square function using Haar basis with $J = 2$. The decomposition coefficients using (9) are: $\alpha^{(2)}$, $\beta^{(2)^i}$, $\beta^{(1)^i}$. The result of applying (14) to $A = \beta^{(1)^D}$, $B_1 = \beta^{(2)^D}$, and $B_2 = \alpha^{(2)}$ has correlation one with A.

**Algorithm 2**

Star Operator for Merging 2D Signals

Require: 2D Signals: $A_{mn}, B_{pq}$

Ensure: Merged 1D Signal: $S_{mn} = A_{mn} * B_{pq}$
1: Convert input signals to 1D signal form: *a, b*
2: Compute: $\gamma = pq/mn \leq 1$
3: Compute: $\Delta = (mn - pq) \geq 1$
4: Generate extension signal $\acute{A}$:
5: Initialize signal $\acute{A}_{(mn(\Delta+1))}$ with all columns equal to *a*
6: Generate extension signal $\acute{B}$:
7: Initialize signal $\acute{B}_{(mn(\Delta+1))}$ with zero element values
8: Fill each column of $\acute{B}$ with values from *b*
9: Each successive column of $\acute{B}$ contains rotated version
10: Compute $\omega_i \in \omega_{(\Delta+1)}$ as correlation between **a** and each column of $\acute{B}$
11: Compute: $\acute{C} = \acute{A} + \omega_i \acute{B}$
12: Compute: *C* as vector norm of each row of $\acute{C}$
13: Compute: $S = \gamma C$

*2.3 DFWT Framework*

*2.3.1 One-dimensional case*

The integrated mathematical representation of one-dimensional forward DFWT is obtained, from Eqs. 3 and 7, as Eq. 16.

$$X_k = (\mathbf{x},\, \mathbf{E}_k) \star ((\mathbf{x},\, \mathbf{E}_{\beta,l}),\, (\mathbf{x},\, \mathbf{E}_{\alpha,J})) \tag{16}$$

Here $p = 2^l m$ for $1 \le l \le J$. Applying (14) with $A = (x, E_k)$, $B_1 = (x, E_{\beta,l})$, and $B_2 = (x, E_{\alpha,J})$:

$$A \star (B_1, B_2) = \frac{m-p+1}{m}((\frac{p}{m}(A \star B_1)) \star B_2) \tag{17}$$

The integrated mathematical representation of one-dimensional inverse DFWT is obtained, from Eqs. 4 and 8, as Eq. 18.

$$\begin{aligned} x_k &= \frac{1}{2}(\frac{(\mathbf{X},\, \mathbf{E}_k)}{N} \circledast \frac{(\alpha_k^{(J)}, \mathbf{E}_{\alpha,J}) + (\beta_k^{(l)}, \mathbf{E}_{\beta,l})}{\sqrt{N}}) \\ &= \frac{1}{2N}((\mathbf{X},\, \mathbf{E}_k) \circledast \sqrt{N}((\alpha_k^{(J)}, \mathbf{E}_{\alpha,J}) + (\beta_k^{(l)}, \mathbf{E}_{\beta,l}))) \end{aligned} \tag{18}$$

The mathematical expressions (18) and (20) used $\circledast$ to show an integrated representation, however, as coefficients in different transform domain representations have different meanings [21]; therefore, the star operator Eqs. 16 and 19 are used to merge coefficients.

*2.3.2 Two-dimensional case*

The integrated mathematical representation of two-dimensional forward DFWT is obtained, from Eqs. 5 and 9, as Eq. 19.

$$\hat{a}_{k,l} = (\mathbf{A},\, \mathbf{E}_{k,l}) \star ((\mathbf{A},\, \mathbf{E}^i_{\beta,l}), (\mathbf{A},\, \mathbf{E}_{\alpha,J})) \tag{19}$$

The integrated mathematical representation of 2D inverse DFWT in (20) is obtained, from Eqs. 6 and 10, as Eq. 20.

$$\begin{aligned} a_{r,s} &= \frac{1}{2}(\frac{(\hat{\mathbf{A}}, \mathbf{E}_{k,l})}{MN} \circledast \frac{(\alpha_k^{(J)}, \mathbf{E}_{\alpha,J}) + (\beta_k^{(l)^i}, \mathbf{E}^i_{\beta,l})}{\sqrt{MN}}) \\ &= \frac{1}{2MN}((\hat{\mathbf{A}}, \mathbf{E}_{k,l}) \circledast \sqrt{MN}((\alpha_k^{(J)}, \mathbf{E}_{\alpha,J}) + (\beta_k^{(l)^i}, \mathbf{E}^i_{\beta,l}))) \end{aligned} \tag{20}$$

## 3. Results and Discussion

The experimental setup includes Dell Inspiron 7577 with Windows 10 operating system and MATLAB R2019a. The signal and image data are from the public domain. Normal heart and early systolic murmur sound signals are from cprworks.com and the ankle image is from [22] website imageprocessingplace.com.

*3.1 DFWT Application*

Many physiological processes have associated signals due their nature and activities [2]. Examples of such signals are biochemical, electrical, and physical. Commonly encountered biomedical signals are electro-cardiogram, electro-encephalogram, phonocardiogram, and vibromyogram. Biomedical imaging captures images of in vivo physiology and physiological processes. Examples are computed tomography scans, ultrasound, and magnetic resonance imaging.

*3.1.1 Merging 1D signals*

The sound signals of normal heart beat and early systolic murmur are shown in Figs. 2 and 4, respectively. Selected sound parts were used to generate the merged sound signal. The normal heart sound signal has 8012 Hz frequency and 30745 data points. From sound data, 800 data points were extracted from 1203 to 2003. The early systolic murmur sound signal has 11025 Hz frequency and 56074 data points. From sound data, 3307 data points were extracted from 8821 to 12127.

The Fourier transform of extracted normal heart sound signal and the wavelet transform of extracted early systolic murmur sound signal were merged using (12). The result is shown in Fig. 4. The use of signal dimension abbreviations 1D and 2D applies to the frequency and wavelet representations. The merged signal patterns may be stored in a dictionary and may be used to develop an application for symptom-specific disease diagnose decision support system.

*3.1.2 Merging 2D signals*

The image data shown in the Fig. 3 was extracted from the DICOM format and resized to 25%. The dimensions of extracted resized image were 64 x 64. Initially, both DFT and DWT were applied on the extracted resized image. Then the Fourier spectrum and approximate coefficients from level one wavelet decomposition were merged.

The application of DFT on extracted resized image generated Fourier spectrum. A patch of size 10 x 10 was extracted from the Fourier spectrum from top-left coordinates (11, 11) to bottom-right coordinates (20, 20). The extracted patch was merged with the level one approximation coefficients with dimension 32 x 32. The result is shown in Fig. 5. In this manner, the proposed formulation may be utilized in an image fusion application – a well-established research discipline.

*3.1.3 Merging 1D and 2D signals*

The diagonal elements were extracted from the Fourier spectrum of extracted resized image to form a 1D signal with 64 elements. The extracted signal is merged with the level one approximation coefficients with dimension

32 x 32 (2D signal). The result is shown in Fig. 6. This result shows the potential of using powerful vector notation that has the ability to transforms a higher dimension signal in 1D signal. This is an essential requirement for the proposed technique.

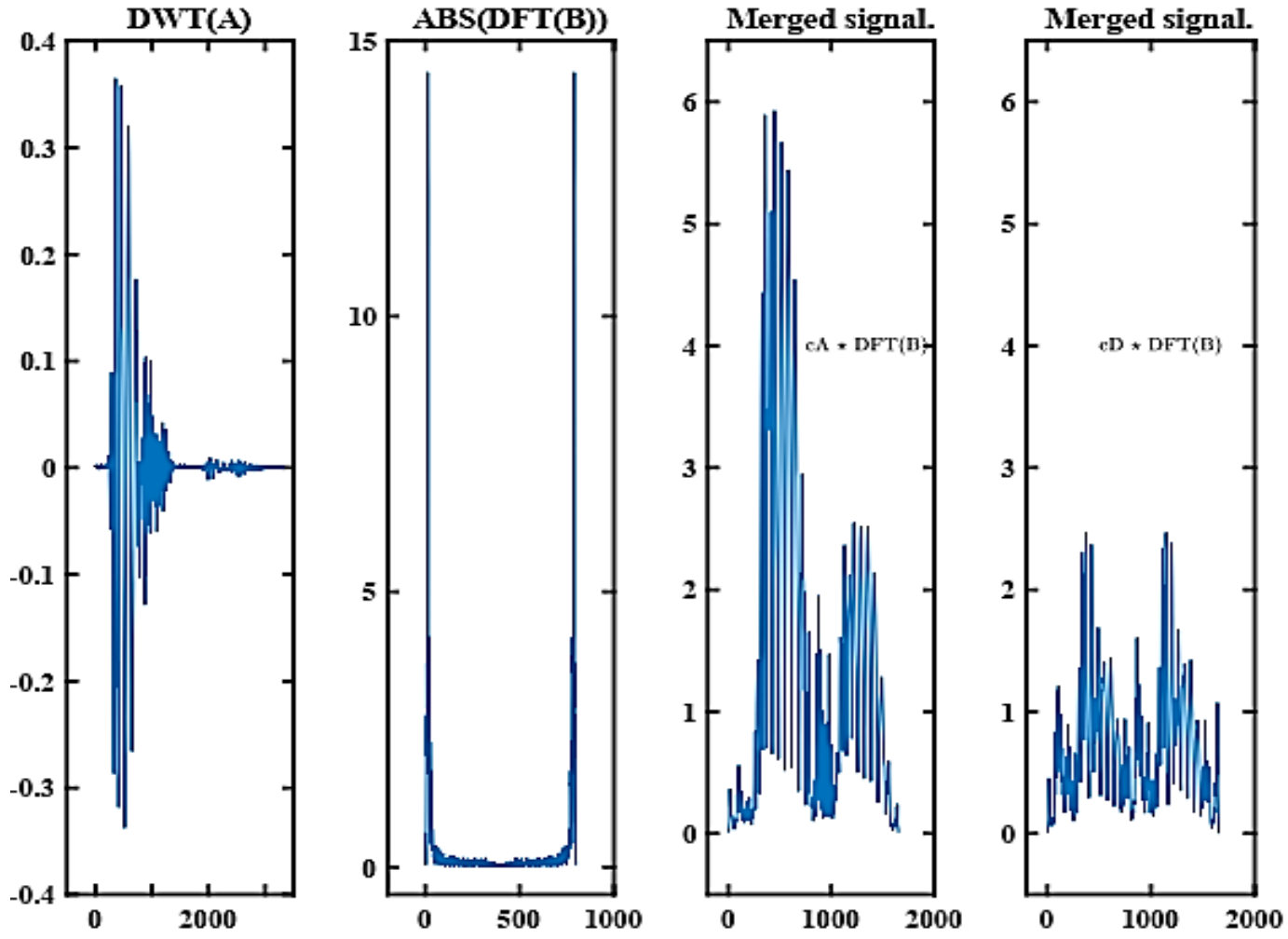


**Fig. 4.** The merged sound signals. From left to right: wavelet decomposition of extracted early systolic murmur sound signal, frequency spectrum of extracted normal heart sound signal, result of merging approximate wavelet coefficients and frequency spectrum, and result of merging detail wavelet coefficients and frequency spectrum. See section 3 for details. Number of data points are shown on x-axis. The amplitude are shown on y-axis

**Fig. 5.** The merged ankle image. From left to right: example ankle MRI input image, frequency spectrum of the resized image, wavelet decomposition of resized image, and result of merging approximate wavelet coefficients and extracted patch from frequency spectrum of the resized image. See section 3 for details

*3.2 Discussion*

The developed star operator in the section 2 is used to formulate the integrated mathematical representation for the DFT and DWT and applied to merge heart sound signals and example MRI image in the section 3. Coefficients from frequency domain and wavelet domain representations are used as input to the star operator Eqs. 12-15. The merging processes in Algorithms 1 and 2 are used for merging 1D signals and 2D signals, respectively.

The mathematical expressions in Eqs. 3, 5, 7 and 9 are derived from [1], [21]. Integrated mathematical expressions for time domain signal and spatial domain image are given in Eqs. 18 and 20, respectively. The star operator Eqs. 16 and 19 is used to merge coefficients from frequency spectrum and wavelet decomposition.

**Fig. 6.** The merged ankle – signal and image merging, See section 3 for details

The application of star operator to compute integrated DFWT representations appeared in Algorithms 1 and 2. In both algorithms, merging achieved through application of the star operator, formulated in the section 2. The demonstration of application appeared in Figs. 4, 5, and 6. The results in Fig. 4 show merging in transform domain representations for the normal heart sound signal and early systolic murmur sound signal. The proposed star operator successfully generated two different representations corresponding to selection of coefficients in the transform domain. Fig. 5 shows another typical merging operation for the example MRI ankle image. The result appeared as a blur version of the input image.

The proposed DFWT framework was successful in generating a composite representation for multiple applications. Furthermore, it has enabled merging 1D signal and 2D signal representations in transform domain. The implementation structure proposed in this paper, however, has the limitation in terms of memory needed during processing. In generating results, the time complexity issue are related to the transformation operations. The standard transformation functions in MATLAB are used for computation. The memory requirements are large to implement the proposed technique due to the use of large 2D signals.

The work accomplished in this study focused on the formulation of an integrated representation for both discrete Fourier transform and discrete Wavelet transform using the powerful vector notation. There are numerous applications that implemented these well-known transformation operations [11, 22]. The proposed formulation in this work, opens another dimension for the exploration possibility.

The proposed formulation is compared with the recent research works [22-26], see Table 1. Javid et al. [22] proposed a fuzzy contrast enhancement system with multiple transform domain operations (FCES-MTDO). Jalayer et al. [23] proposed a multi-domain convolutional long short-term memory (MD-CLSTM) to generate fault signatures for fault detection and diagnosis of rotating machinery. Chaudhary et al. [24] used a two-dimensional Fourier-Bessel series expansion-based empirical wavelet transform (2D-FBSE-EWT) to automate the glaucoma diagnosis from medical images. Li et al. [25] proposed a double-encrypted watermarking algorithm based on cosine transform and fractional Fourier transform in invariant wavelet domain (DEWA-CTFFT). You et al. [26] combined Fourier-wavelet transforms for studying the dynamic response of anisotropic multi-layered flexible pavement with linear-gradual interlayers (DR-AMFP-LGI).

## 4. Conclusion

An integrated mathematical formulation for the discrete Fourier transform and the wavelet transform has been presented. The proposed framework has been applied successfully to merge biomedical signals and images. The developed star operator was successful in merging transform domain representations. Furthermore, the star operator enabled merging data from different input domains, that is, one input from the time domain signal and another input from the image domain. The proposed

technique utilized powerful vector notation to convert input data to vector form and compute the integrated transformation. Possible future research directions include exploring merging higher dimensional data, using fuzzy logic to integrate FFT and FWT in a single application, explore the application of integrated transformation for data fusion, and developing a computational approach to overcome the memory limitation experienced in implementation of the star operator.

**Table 1**

Comparison of the proposed technique with recent research works

| Technique | Signal | Image | Multi-domain | Vector notation | Implementation | Application |
|---|---|---|---|---|---|---|
| FCES-MTDO [22] | No | Yes | Yes | No | Parallel | Image fusion |
| MD-CLSTM [23] | Yes | No | Yes | No | Parallel | Fault signature |
| 2D-FBSE-EWT [24] | No | Yes | Yes | No | Serial | Object detection |
| DEWA-CTFFT [25] | No | Yes | Yes | No | Serial | Watermarking |
| DR-AMFP-LGI [26] | No | Yes | Yes | No | Serial | Structural design |
| Proposed Technique | Yes | Yes | Yes | Yes | Integrated | Signal merging |

## 5. Acknowledgment

Authors would like to acknowledge Hamdard University for the research grant no. HURC-16-048/2017.

## 6. References

[1] A. S. Broughton and K. Bryan, "Discrete Fourier Analysis and Wavelets: Applications to Signal and Image Processing", Wiley New York USA, 2018.

[2] R. M. Rangayyan, "Biomedical Signal Analysis", IEEE New Jersey USA, 2015.

[3] M. Vetterli, J. Kovacevic, and V. K. Goyal, "Foundations of Signal Processing", MIT Press USA, 2014.

[4] D. Baleanu, "Wavelet Transforms and Their Recent Applications in Biology and Geoscience", IntechOpen Hague Netherlands, 2012.

[5] S. Mallat, "A Wavelet Tour of Signal Processing: The Sparse Way", Academic Press Burlington MA USA, 2008.

[6] S. Mallat, "A Theory for Multiresolution Signal Decomposition: The Wavelet Representation", IEEE Transactions on Pattern Anlysis and Machine Intelligence, vol. 11, no. 7, pp. 674–693, 1989.

[7] Y. Sheng, "Wavelet Transform", in Transforms and Applications Handbook, CRC Press USA, 2010.

[8] S. Araghinejad, "Data-driven Modeling: Using MATLAB in Water Resources and Environmental Engineering", Springer Dordrecht Netherlands, 2014.

[9] M. Ali, C. V. Ahn, and M. Pant, "An Efficient Lossless Robust Watermarking Scheme by Integrating Redistributed Invariant Wavelet and Fractional Fourier Transforms", Multimedia Tools and Applications, vol. 77, no. 10, pp. 1–23, 2017.

[10] W. H. Khoh, T. S. Ong, Y. H. Pang, and A. B. J. Teoh, "Score Level Fusion Approach in Dynamic Signature Verification based on Hybrid Wavelet-Fourier Transform", Security and Communication Networks, vol. 7, no. 7, pp. 1067–1078, 2014.

[11] A. Majumdar, R. K. Ward, and T. Aboulnasr, "Compressed Sensing based Real-Time Dynamic MRI Reconstruction", IEEE Transactions on Medical Imaging, vol. 31, no. 12, pp. 2253–2266, 2012.

[12] M. Lustig, D. Donoho, and J. M. Pauly, "Sparse MRI: The Application of Compressed Sensing for Rapid MR Imaging", Magnetic Resonance in Medicine, vol. 58, no. 6, pp. 1182–1195, 2007.

[13] D. L. Donoho, "Compressed Sensing", IEEE Transactions on Information Theory, vol. 52, no. 4, pp. 1289–1306, 2006.

[14] R. X. Gao and R. Yan, "Wavelets: Theory and Applications for Manufacturing", Springer New York USA, 2010.

[15] G. Chen, "Automatic EEG Seizure Detection using Dual-Tree Complex Wavelet-Fourier Features", Expert Systems with Applications, vol. 41, no. 5, pp. 2391–2394, 2014.

 

[16] B. Munch, P. Trtik, F. Marone, and M. Stampanoni, “Stripe and Ring Artifact Removal with Combined Wavelet-Fourier Filtering”, Optics Express, vol. 17, no. 10, pp. 8567–8591, 2009.

[17] T. Tarasiuk, “Hybrid Wavelet-Fourier Spectrum Analysis”, IEEE Transactions on Power Delivery, vol. 19, no. 3, pp. 957–964, 2004.

[18] T. J. Ali, P. Akhtar, M. Faris, I. Mala, and S. S. Zia, “Implementation of Discrete Fourier Transform and Orthogonal Discrete Wavelet Transform in Python”, Journal of Independent Studies and Research – Computing, vol. 14, no. 1, pp. 1–11, 2016.

[19] D. Sundararajan, "Discrete Wavelet Transform: A Signal Processing Approach", Wiley Singapore, 2015.

[20] T. Xiao, S. Hu, and Y. Xiao, “2-D Hybrid Wavelet-Fourier Transformation”, 8th International Conference on Signal Processing, Guilin China, vol. 1, pp. 109-111, 2006.

[21] R. C. Gonzalez and R. E. Woods, "Digital Image Processing", Pearson New York USA, 2018.

[22] T. Javid and M. Abid, “Fuzzy Contrast Enhancement System with Multiple Transform Domain Operations”, Advances in Electrical and Computer Engineering, vol. 21, no. 1, pp. 83-90, 2021.

[23] M. Jalayer, C. Orsenigo, and C. Vercellis, “Fault Detection and Diagnosis for Rotating Machinery: A Model based on Convolutional LSTM, Fast Fourier and Continuous Wavelet Transforms”, Computers in Industry, vol. 125, p. 103378, 2021.

[24] P. K. Chaudhary and R. B. Pachori, “Automatic Diagnosis of Glaucoma using Two-Dimensional Fourier-Bessel Series Expansion based Empirical Wavelet Transform”, Biomedical Signal Processing and Control, vol. 64, p. 102237, 2021.

[25] Y. M. Li, D. Wei, and L. Zhang, "Double-Encrypted Watermarking Algorithm based on Cosine Transform and Fractional Fourier Transform in Invariant Wavelet Domain", Information Sciences, vol. 551, pp. 205-227, 2021.

[26] L. You, J. Man, K. Yan, D. Wang, and H. Li, “Combined Fourier-Wavelet Transforms for Studying Dynamic Response of Anisotropic Multi-Layered Flexible Pavement with Linear-Gradual Interlayers”, Applied Mathematical Modelling, vol. 81, pp. 559-581, 2020.

 